INTERNATIONAL JOURNAL OF UROLOGY

International Journal of Urology (2013) 20, 468–477 doi: 10.1111/j.1442-2042.2012.03182.x

Original Article: Clinical Investigation

MicroRNA-155 is a predictive marker for survival in patients with clear cell renal cell carcinoma

Shunsuke Shinmei,[1,2] Naoya Sakamoto,[1] Keisuke Goto,[1,2] Kazuhiro Sentani,[1] Katsuhiro Anami,[1] Tetsutaro Hayashi,[2] Jun Teishima,[2] Akio Matsubara,[2] Naohide Oue,[1] Yasuhiko Kitadai[3] and Wataru Yasui[1]

Departments of [1]Molecular Pathology, [2]Urology and [3]Medicine and Molecular Science, Hiroshima University Graduate School of Biomedical Sciences, Hiroshima, Japan

Abbreviations & Acronyms
AJCC = American Joint Committee on Cancer
ccRCC = clear cell renal cell carcinoma
cDNA = complementary deoxyribonucleic acid
CFS = cancer-free survival
CI = confidence intervals
CSS = cancer-specific survival
FFPE = formalin fixed paraffin embedded
HIF-1α = hypoxia-inducible factor-1α
HR = hazard ratio
IFN-α = interferon-α
IHC = immunohistochemistry
miRNA = micro-ribonucleic acid
NS = not significant
PI3K = phosphoinositide 3-kinase
qRT–PCR = quantitative reverse transcription polymerase chain reaction
RCC = renal cell carcinoma
RNA = ribonucleic acid
SE = standard error

Correspondence: Wataru Yasui M.D., Ph.D., Department of Molecular Pathology, Hiroshima University Graduate School of Biomedical Sciences, 1-2-3 Kasumi, Minami-ku, Hiroshima 734-8551, Japan. Email: wyasui@hiroshima-u.ac.jp

Received 9 March 2012; accepted 5 September 2012. Online publication 10 October 2012

Objectives: To investigate the clinical significance of micro-ribonucleic acid-155 in clear cell renal cell carcinoma, in particular focusing on the association of expression levels of micro-ribonucleic acid-155 with clinicopathological factors, cancer-specific survival and therapeutic outcomes in clear cell renal cell carcinoma patients.

Methods: Quantitative reverse transcription polymerase chain reaction of micro-ribonucleic acid-155 was carried out on 137 clear cell renal cell carcinoma cases, containing 77 matched pairs of clear cell renal cell carcinoma and normal adjacent kidney tissues from the same patients.

Results: Significant overexpression of micro-ribonucleic acid-155 was found in clear cell renal cell carcinoma compared with normal kidney tissue. Expression of micro-ribonucleic acid-155 was not associated with prognosis in all stage groups. However, in 43 patients with stage III and IV clear cell renal cell carcinoma, low expression levels of micro-ribonucleic acid-155 correlated with a poor prognosis. Regarding cancer-free survival of 26 patients with stage III and IV clear cell renal cell carcinoma who received curative resection and cancer-specific survival of 31 patients who received postoperative therapy with interferon-α after radical nephrectomy, low expression levels of micro-ribonucleic acid-155 correlated with poor clinical outcomes in these two groups.

Conclusions: Low expression of micro-ribonucleic acid-155 represents a valuable marker of poor clinical outcomes in patients with stage III and IV clear cell renal cell carcinoma.

Key words: hypoxia-inducible factor-1α, micro-ribonucleic acid, micro-ribonucleic acid-155, quantitative reverse transcript polymerase chain reaction, renal cell carcinoma.

Introduction

RCC is the most common neoplasm of the adult kidney and the incidence is increasing worldwide, and the most common subtype is ccRCC.[1] If detected early, ccRCC can be treated surgically, and 5-year survival rates approaching 85% can be achieved for patients with organ-confined disease.[2] In reality, 40–50% of patients develop metastatic disease; 20–30% present with metastases, and 20–30% relapse distantly after curative nephrectomy. Treatment options for these patients are limited, and expected 5-year survival is approximately 10%.[2] Therefore, it is necessary to identify new biomarkers enabling prediction of early metastasis after nephrectomy and to develop new targeted therapies.

MiRNA are short non-coding RNA of 18–25 nucleotides in length that regulate gene expression post-transcriptionally. Aberrant miRNA expression is reported in many cancers, suggesting that they have a novel role as oncogenes or tumor suppressors.[3–5] Recent evidence showed the diverse clinical uses of miRNA for cancer as diagnostic, prognostic and predictive markers.[6] Differential expression of miRNA has been investigated in RCC. MiR-122, miR-155, miR-21, miR-106a, miR-182, miR-106b and miR-210 have been

reported to be overexpressed in RCC, whereas miR-141, miR-200c, miR-335 and miR-218 are downregulated.[7–15] MiR-155 has repeatedly been identified through miRNA microarray profiling as upregulated in RCC tissue and its biological role has been studied.[11,12] A significant correlation was found between miR-155 expression and tumor size.[7,8,16] Although miR-155 correlates with prognosis in breast cancer, lung cancer, hepatocellular carcinoma, colorectal cancer and pancreatic tumors,[17–21] there is only one report examining the correlation between miR-155 and prognosis in ccRCC, which was analyzed in just 31 cases and showed no prognostic impact of miR-155.[8] To confirm the correlation between miR-155 and prognosis of ccRCC patients, more validation studies in large sample sets should be carried out.

In the present study, we analyzed expression levels of miR-155 in 137 ccRCC cases by qRT–PCR, and compared these to the expression levels from 77 corresponding normal kidney tissue samples. Furthermore, the associations between expression levels of miR-155 and clinicopathological factors including prognosis were also investigated.

Methods

Tissue samples

In total, 137 primary tumor samples and 77 normal adjacent samples were collected from patients diagnosed with ccRCC. Patients were treated at the Hiroshima University Hospital from 1993 to 2010. Some cases, from a single institution, that did not have available tissue and clinical information about postoperative follow up were excluded.

Clinical stage was determined according to the AJCC Cancer Staging Manual, 7th edition. Patient's ages ranged between 34 and 89 years, with a median of 66 years. Histological diagnosis was established according to the guidelines of the World Health Organization. Cases were selected according to tissue availability and were not stratified for any known preoperative or pathological prognostic factor. The median follow-up time for all cases was 65 months and ranged from 2 to 188 months. We measured tumor sizes in 123 ccRCC tissue samples that could be confirmed macroscopically in pathological samples.

Because written informed consent was not obtained, for strict privacy protection the identifying information for all samples was removed before analysis. This procedure was in accordance with the Ethical Committee for Human Genome Research of Hiroshima University (Hiroshima, Japan). Clinical details of the patients are summarized in Table 1. We analyzed 43 samples to confirm stage III and IV in 137 samples. The patient's clinical details are summarized in Table 2.

For qRT–PCR, 137 ccRCC samples and 77 corresponding normal adjacent samples were used. Samples were FFPE tissues from 137 patients who had undergone surgical excision for ccRCC.

MiRNA extraction and qRT–PCR

MiRNA was extracted using a RecoverAll Total Nucleic Acid Isolation Kit for FFPE tissues (Ambion, Foster City, CA, USA). Reverse transcription was carried out using a TaqMan microRNA reverse transcription kit (Applied Biosystems, Foster City, CA, USA) according to the manufacturer's protocol. Hsa-miR-155 was detected using TaqMan MicroRNA assays (Assay ID 000479; Applied Biosystems). Real-time quantification of cDNA was carried out on a 7900HT Fast Real-Time PCR System (Applied Biosystems). Expression data were normalized according to expression of the RNU48 reference DNA (Assay ID 001006; Applied Biosystems).[22]

Immunohistochemistry

IHC was carried out on 4-μm thick sections of FFPE. Immunohistochemical analysis was carried out with a Dako EnVision+ System- HRP Labelled Polymer anti-mouse (Dako Cytomation, Carpinteria, CA, USA). Antigen retrieval for HIF-1α was carried out by microwave heating in citrate buffer (pH 6.0) for 30 min. After peroxidase activity had been blocked with 1% H_2O_2 / 50% methanol for 10 min, HIF-1α was detected with a mouse monoclonal antibody Mab H1α67 (1:200; Novus Biologicals, Littleton, CO, USA). A total of 64 sections were incubated with primary antibody for 1 h at room temperature, and then with Dako EnVision+ System- HRP Labelled Polymer anti-mouse for 1 h. For color reaction, sections were incubated with 3,3′-diaminobenzidine Substrate-Chromogen Solution (Dako Cytomation) for 3 s. Sections were counterstained with 0.1% hematoxylin. The cut-off point for antibody reactivity necessary to define a result as positive was staining of any cells with nuclear localization in surgically resected specimens.

IHC was carried out on 64 ccRCC samples, including 39 with the lowest expression of miR-155 tissue and 25 with the highest expression of miR-155 tissues of 137 patients who had undergone surgical excision for ccRCC.

Statistical analysis

Statistical differences between miRNA expression levels in ccRCC samples and normal kidney samples were evaluated using the Wilcoxon matched pairs test. Statistical differences of RNU48 reference DNA were evaluated using the non-parametric Mann–Whitney *U*-test. For analysis of correlation between expression levels of miR-155 and tumor size, we used the non-parametric Spearman's rank correlation coefficient. The correlation between expression levels

Table 1 Clinical characteristics of the 137 ccRCC patients

			Expression of miR-155		*P*-value
			Low	High	
Sex (%)		Sex (%)			0.0426
Male	103 (75)	Male	103 (75)	46	57
Female	34 (25)	Female	34 (25)	22	12
Side (%)		Side (%)			NS
Left	59 (43)	Left	59 (43)	24	35
Right	78 (57)	Right	78 (57)	44	34
Median age, years (range)		Median age, years (%)			NS
	66 (34–89)	<65	64 (47)	34	30
		≥65	73 (53)	34	39
Histological grade (%)		Histological grade (%)			NS
G1	60 (44)	G1–2	103 (75)	56	47
G2	43 (31)	G3–4	34 (25)	12	22
G3	31 (23)				
G4	3 (2)				
Infiltrating type (%)		Infiltrating type (%)			NS
INFa	113 (82)	INFa	113 (82)	57	56
INFb	23 (17)	INFb/c	24 (18)	11	13
INFc	1 (1)				
pT stage (%)		pT stage (%)			NS
pT1	83 (61)	pT1–2	99 (72)	52	47
pT2	16 (12)	pT3–4	38 (28)	16	22
pT3	36 (26)				
pT4	2 (1)				
pN stage (%)		pN stage (%)			NS
pNx	79 (58)	pNx/0	129 (94)	66	63
pN0	50 (36)	pN1/2	8 (6)	2	6
pN1/2	8 (6)				
Venous invasion (%)		Venous invasion (%)			NS
v0	93 (68)	v0	93 (68)	49	44
v1	44 (32)	v1	44 (32)	19	25
M stage (%)		M stage (%)			NS
M0	117 (85)	M0	117 (85)	60	57
M1	20 (15)	M1	20 (15)	8	12
Stage grouping (%)		Stage grouping			NS
Stage I	81 (59)	Stage I/II	94 (68)	50	44
Stage II	13 (9)	Stage III/IV	43 (32)	18	25
Stage III	23 (17)				
Stage IV	20 (15)				
Observation period (months)					
Median	65				
Range	2–188				

The expression levels of miR-155 were divided into two groups, low and high expression of miR-155, based on the median miR-155 expression level (cut-off line = the median miR-155 expression level in this group). Corresponding median value = –0.0831.

of miR-155, clinicopathological parameters and expression of HIF-1α in IHC was analyzed with Fisher's exact test. A log–rank test and Kaplan–Meier plots were constructed for the miR-155-high and miR-155-low groups. Univariate and multivariate analysis of factors influencing survival were carried out using the Cox proportional hazards model. And parameters at multivariate analysis were selected by the stepwise method. The HR and 95% CI were estimated from

Table 2 Clinical characteristics of 43 stage III and IV ccRCC patients

				Expression of miR-155	*P*-value
				Low / High	
Sex (%)		Sex (%)			NS
Male	39 (90)	Male	39 (90)	18 / 21	
Female	4 (10)	Female	4 (10)	3 / 1	
Side (%)		Side (%)			NS
Left	14 (33)	Left	14 (33)	6 / 8	
Right	29 (67)	Right	29 (67)	15 / 14	
Median age, years (range)		Median age, years (%)			NS
	66 (45–89)	<65	21 (49)	10 / 11	
		≥65	22 (51)	11 / 11	
Histological grade (%)		Histological grade (%)			NS
G1	7 (16)	G1–2	22 (59)	11 / 11	
G2	15 (35)	G3–4	21 (51)	11 / 10	
G3	18 (42)				
G4	3 (7)				
Infiltrating type (%)		Infiltrating type (%)			NS
INFa	25 (58)	INFa	25 (58)	13 / 12	
INFb	17 (40)	INFb/c	18 (42)	8 / 10	
INFc	1 (3)				
pT stage (%)		pT stage (%)			NS
pT1	2 (5)	pT1–2	5 (12)	3 / 2	
pT2	3 (7)	pT3–4	38 (88)	18 / 20	
pT3	36 (84)				
pT4	2 (5)				
pN stage (%)		pN stage (%)			NS
pNx	7 (16)	pNx/0	35 (81)	17 / 18	
pN0	28 (65)	pN1/2	8 (19)	4 / 4	
pN1/2	8 (19)				
Venous invasion (%)		Venous invasion (%)			NS
v0	8 (19)	v0	8 (19)	5 / 3	
v1	35 (81)	v1	35 (81)	16 / 19	
M stage (%)		M stage (%)			NS
M0	23 (53)	M0	23 (53)	10 / 13	
M1	20 (47)	M1	20 (47)	11 / 9	
Observation period (months)					
Median	43				
Range	2–188				

The expression levels of miR-155 were divided into two groups, low and high expression of miR-155, based on the median miR-155 expression level (cut-off line = the median miR-155 expression level in this group). Corresponding median value = −0.0811.

the Cox proportional hazard model. Wilcoxon matched pairs test, Pearson's product-moment correlation coefficient, Fisher's exact test, a log–rank test and Kaplan–Meier plots were calculated using JMP software version 10 (SAS Institute, Cary, NC, USA). The Cox proportional hazards model, stepwise method and concordance, R^2 and Wald test were calculated using the R statistical environment (http://www.R-project.org). For all analyses, age was treated as a categorical variable (65 years or more *vs* less than 65 years). A *P*-value of less than 0.05 was considered statistically significant.

Results

Expression levels of miR-155 between ccRCC and normal kidney tissues

We analyzed 77 matched pairs of ccRCC and normal adjacent kidney tissues from the same patients by qRT–PCR. To

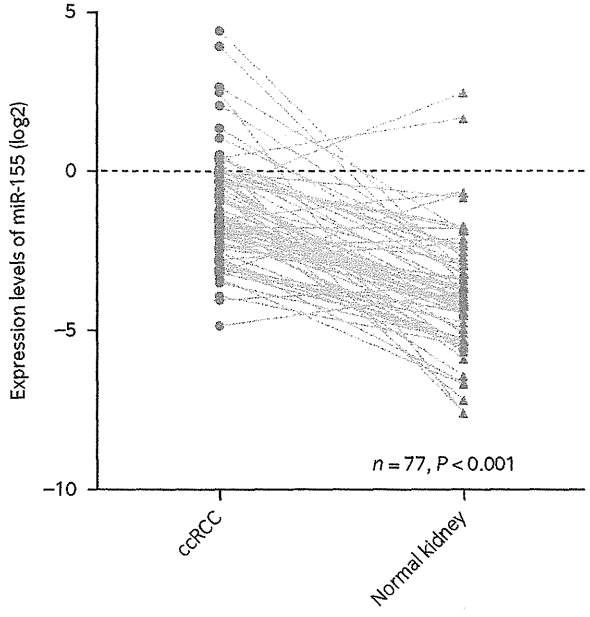

Fig. 1 Expression of miR-155 between tumor and normal kidney tissue in 77 ccRCC samples in all stages ($P < 0.001$).

show the usefulness of RNU48 as a reference gene, we analyzed the expression of RNU48 between tumors and normal adjacent kidney tissue in 77 matched pairs of ccRCC samples (Fig. S1a). The expression level of RNU48 in some clinicopathological parameters in 137 ccRCC samples was also examined (Fig. S1b). The expression level of RNU48 showed no significant difference between tumors and normal adjacent kidney, and also among all clinicopathological parameters. Therefore, we confirmed that RNU48 is stably expressed in ccRCC and is useful as a reference gene.

Differences between the two groups were evaluated using the Wilcoxon matched pairs test. Highly significant differences were identified between 77 ccRCC with all stages and normal adjacent kidney tissues in the expression levels of miR-155 ($P < 0.001$), as well as limited to 63 ccRCC with stage I and II ($P < 0.001$), and 14 ccRCC with stage III and IV ($P = 0.0138$; Fig. 1).

Relationship between miR-155 expression and tumor size

We analyzed the correlation between expression levels of miR-155 and tumor size in 123 ccRCC tissues in which the tumor sizes had been established. Tumor size ranged between 0.8 and 17 cm, with a median of 4.6 cm. For analysis of the correlation between expression levels of miR-155 and tumor size, we used the non-parametric Spearman's rank correlation coefficient. There were no statistically significant differences, but expression levels of miR-155 tended to be associated with a tumor size ($r = 0.2045$, $P = 0.0943$; Fig. 2).

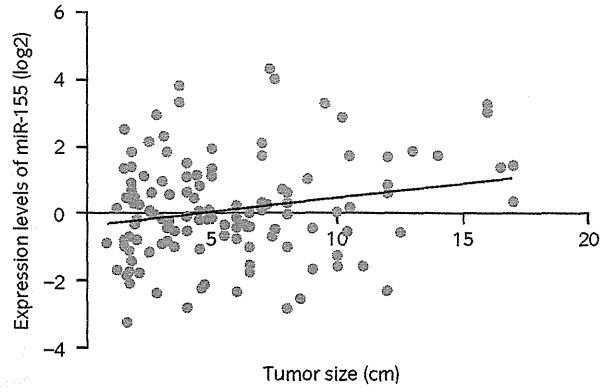

Fig. 2 Correlation between expression levels of miR-155 and tumor size in 123 samples. Pearson's product-moment correlation coefficient 0.2045 ($P = 0.0943$).

Expression levels of miR-155 and clinical prognosis

To determine the difference in CSS and CFS on the basis of expression levels of miR-155, we divided the sample into two groups (low and high expression levels of miR-155) based on the median miR-155 expression level in the group. Kaplan–Meier plots were constructed in 137 ccRCC with all stages. This analysis showed no association with prognosis ($P = 0.7001$; Fig. 3a). In contrast, when limited to the stage III and IV groups, the analysis showed significant differences for CSS on the basis of miR-155 expression levels; low expression levels of miR-155 were correlated with poor prognosis in Kaplan–Meier plots and log–rank tests ($P = 0.0337$; Fig. 3b). Regarding the CFS of 26 patients with stage III and IV ccRCC who had received curative resection, means status of no visible residual tumor clinically after radical nephrectomy with or without metastatectomy. Low expression levels of miR-155 tended to be associated with a high rate of recurrence ($P = 0.0614$; Fig. 3c). We also analyzed CSS in 31 patients who had received postoperative IFN-α therapy after radical nephrectomy, and found that low expression levels of miR-155 were associated with poor prognosis ($P = 0.0464$; Fig. 3d).

Univariate and multivariate analysis of factors influencing survival

In univariate analyses, M stage, histological grade, infiltrating type, pT stage and pN stage were correlated with poor prognosis. Although high expression levels of miR-155 in univariate analysis were not correlated with poor prognosis, the independent predictors in the multivariate analysis were M stage, pT stage, pN stage and low expression levels of miR-155 (Table 3). In univariate analysis confined to patients with stage III and IV ccRCC, M stage, pN stage and low expression levels of miR-155 were correlated with poor

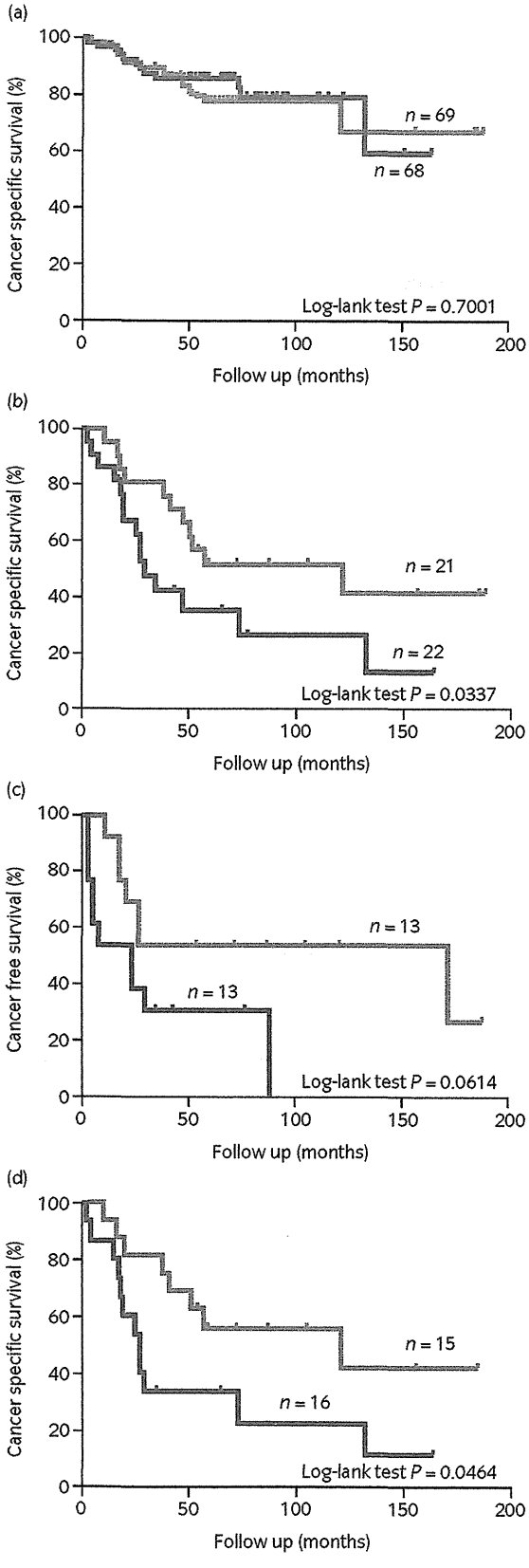

Fig. 3 (a) CSS of 137 patients with ccRCC based on the expression levels of miR-155 (cut-off line = the median miR-155 expression level in this group). Corresponding median value = –0.0831; $P = 0.7001$. (b) CSS of 43 patients with ccRCC based on the expression levels of miR-155 (cut-off line = the median miR-155 expression level in this group) in stage III and IV. Corresponding median value = –0.0811; $P = 0.0337$. (c) CFS of 26 patients after undergoing curative resection for ccRCC based on the expression levels of miR-155 (cut-off line = the median miR-155 expression level in this group) in stage III and IV. Corresponding median value = 0.6190; $P = 0.0614$. (d) CSS of 31 patients with ccRCC based on expression levels of miR-155 (cut-off line = the median miR-155 expression level in this group) in 31 patients who received postoperative therapy with IFN-α after radical nephrectomy. Corresponding median value = 0.59781; $P = 0.0464$. ——, miR-155 high; ——, miR-155 low.

prognosis. Independent predictors in multivariate analysis were M stage, histological grade, pT stage and low expression levels of miR-155. These experiments yielded that low expression of miR-155 was an independent indicator of poor prognosis (Table 4).

Relationship between HIF-1α expression and expression of miR-155

We used IHC to investigate the association between HIF-1α expression and expression of miR-155 in 64 ccRCC samples that included 39 lowest expression of miR-155 tissue and 25 highest expression of miR-155 tissues in the 137 samples we analyzed.

In the 39 low expression levels of miR-155 ccRCC, the HIF-1α positive and HIF-1α negative tumor frequency were 17 out of 39 (44%) and 22 out of 39 (56%). In contrast, in the 25 high expression of miR-155 ccRCC, the HIF-1α positive and HIF-1α negative tumor frequency were 17 out of 25 (66%) and eight out of 25 (32%; Fig. 4). For analysis of the correlation between expression of miR-155 and HIF-1α, we used the Fisher's exact test. This difference was not statically significant, but high expression levels of miR-155 tended to be associated with a high HIF-1α expression ($P = 0.0744$; Table 5).

Discussion

RCC remains to be one of the leading causes of death, so finding new molecular targets for its diagnosis, prognosis and treatment has the potential to improve the clinical strategies and outcomes of this disease. One of the most frequently studied miRNA in cancer biology, miR-155, has also been repeatedly identified through miRNA microarray profiling as upregulated in ccRCC tissue. It has been

Table 3 Univariate and multivariate analysis of factors influencing survival in 137 patients with ccRCC

	Univariate analysis			Multivariate analysis			
	Hazard ratio	95% CI	*P*-value	Hazard ratio	95% CI	Robust SE	*P*-value
Sex							
Female	1		0.0539	Non-selected			
Male	4.12	0.98–17.42					
Age (years)							
<65	1		0.411	Non-selected			
≥65	1.01	0.98–1.05					
Side							
Right	1		0.9930	1		0.612	0.1500
Left	1.01	0.46–2.17		2.44	0.73–8.10		
M stage							
cM0	1		<0.0001	1		0.485	<0.0001
cM1	18.31	8.18–41.02		8.6	3.33–22.25		
Histological grade							
G1/2	1		<0.0001	1		0.608	0.0710
G3/4	5.30	2.46–11.42		3.00	0.91–9.99		
INF							
INF a	1		<0.0001	Non-selected			
INF b/c	6.51	3.02–14.08					
pT							
pT1/2	1		<0.0001	1		0.959	0.0055
pT3/4	19.73	6.77–57.52		14.37	2.19–94.17		
pN stage							
pNx/0	1		<0.0001	1		0.461	0.0380
pN1/2	10.68	4.33–26.38		2.60	1.05–6.42		
Expression of miR-155							
High (>median)	1		0.9850	1		0.421	0.0001
Low (≤median)	0.99	0.47–2.11		5.49	2.40–12.52		

Concordance = 0.946 (SE = 0.059), R^2 = 0.493, Wald test = 52.93 on 6 d.f. (P < 0.0001).

reported that miR-155 levels are almost 30-fold higher in ccRCC compared with normal tissues.[16] Consistent with this result, our qRT–PCR analysis showed that expression levels of miR-155 were 6.2-fold higher in 77 matched pairs of ccRCC than in normal adjacent kidney tissues (P < 0.001). The correlation between high expression levels of miR-155 and tumor size in ccRCC has been reported,[7,8] and we also confirmed a significant association between expression of miR-155 and tumor size (r = 0.2045, P = 0.0238). The available experimental evidence indicates that miR-155 is overexpressed in a variety of malignant tumors. MiR-155 behaves as an oncogenic miRNA in breast cancer, lung cancer, hepatocellular carcinoma, colorectal cancer and pancreatic tumors.[17–21] It has been reported that miR-155 downregulates many tumor suppressor genes that repress PI3K or apoptosis-related signaling.[17,23,24] MiR-155 can be attributed to ccRCC tumor progression.

A significant correlation was found between low expression levels of miR-155 and prognosis in 43 patients with stage III and IV ccRCC using the log–rank test, and univariate and multivariate analysis. Especially in multivariate analysis, low expression levels of miR-155 showed a strong correlation with poor prognosis (P = 0.0010), and the CFS of 26 patients who had received curative resection tended to be associated with low expression levels of miR-155. We also found a significant correlation between low expression levels of miR-155 and prognosis in 31 patients who had received postoperative therapy with IFN-α after radical nephrectomy. These results are inconsistent with the results of all 137 cases. In general, the central part of a tumor will be in an ischemic and hypoxic state. Tumor cells undergo a variety of biological responses when placed in hypoxic conditions, including activation of signaling pathways that regulate proliferation, angiogenesis and cell death by the transcription factor HIF-1α.[25] The overexpression of HIF-1α is one of the important characteristic genetic abnormalities in ccRCC.[26] It has also been reported that hypoxia-induced miR-155 plays a role as a component of a network of negative feedback loops that controls HIF-1α translation.[27] It is well known that HIF-1α overexpression is a

Table 4 Univariate and multivariate analysis of factors influencing survival in 43 patients with stage III and IV ccRCC

	Univariate analysis			Multivariate analysis			
	Hazard ratio	95% CI	*P*-value	Hazard ratio	95% CI	Robust SE	*P*-value
Sex							
Female	1		0.6570	Non-selected			
Male	1.38	0.33–5.89					
Age (years)							
<65	1		0.4260	Non-selected			
≥65	1.01	0.98–1.05					
Side							
Right	1		0.0673	1		0.584	0.1700
Left	2.11	0.46–2.17		0.45	0.14–1.41		
M stage							
cM0	1		0.0020	1		0.452	<0.0001
cM1	3.69	1.61–8.48		11.56	4.77–28.01		
Histological grade							
G1/2	1		0.0611	1		0.531	0.0110
G3/4	2.13	0.97–4.71		3.88	1.37–10.97		
INF							
INFa	1		0.0947	Non-selected			
INFb/c	1.90	0.86–4.01					
pT							
pT1/2	1		0.9210	1		0.685	<0.0001
pT3/4	1.06	0.32–3.57		22.55	5.88–86.41		
pN stage							
pNx/0	1		0.0433	1		0.574	0.1300
pN1/2	2.54	1.03–6.27		2.39	0.78–7.37		
Expression of miR-155							
High (>median)	1		0.0384	1		0.389	0.0001
Low (≤median)	2.31	1.05–5.11		4.67	2.18–10.00		

Concordance = 0.818 (SE = 0.063), $R^2 = 0.561$, Wald test = 27.42 on 6 d.f. ($P = 0.0001$).

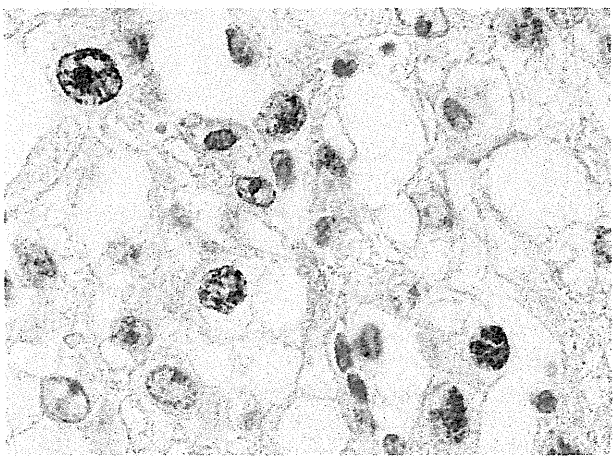

Fig. 4 IHC staining for HIF-1α in ccRCC. HIF-1α immunoreactivity in nuclei of tumor cells.

Table 5 Association between expression of HIF-1α and expression of miR-155 ($P = 0.0744$)

	Expression of miR-155		*P*-value
	Low, ($n = 39$)	High, ($n = 25$)	
	n (%)	*n* (%)	
HIF-1α			
Positive	17 (44%)	17 (68%)	0.0744
Negative	22 (56%)	8 (32%)	

marker of unfavorable prognosis in human cancers and increases with tumor size.[26,28–30] Based on the results of the present study, miR-155 is expressed with increasing tumor size, much as HIF-1α. Consistent with these results and past reports, expression of HIF-1α also tended to be more frequently found in ccRCC cases with high expression levels of

miR-155 in IHC ($P = 0.0720$). In 137 ccRCC of all stages, there were no associations with prognosis in Kaplan–Meier plots, because this group includes many small tumor cases where it is suspected that there is a low expression of both HIF-1α and miR-155. However, when limited to the stage III and IV ccRCC groups, low expression levels of miR-155 showed a strong correlation with poor prognosis in Kaplan–Meier plots. This group includes many large tumor cases where it is suspected that both HIF-1α and miR-155 are highly expressed. It is suspected that expression of miR-155, in part, suppressed by certain factors might lead to breaking the state of the negative feedback loop and accumulation of HIF-1α, and worsening of the prognosis. Further study should be carried out to clarify which factors downregulate expression of miR-155 in advanced ccRCC showing poor prognosis.

In summary, the present study showed that miR-155 was significantly upregulated in ccRCC compared with normal tissue, and high expression levels of miR-155 were correlated with increased tumor size. We also identified that the expression of miR-155 was significantly suppressed in patients with stage III and IV ccRCC and was associated with poor prognosis. Thus, miR-155 might be a valuable biomarker for predicting the survival of patients with stage III and IV RCC, and play an important role in ccRCC progression.

Acknowledgments

We thank Mr Shinichi Norimura for his excellent technical assistance and advice. This work was carried out with the kind cooperation of the Research Center for Molecular Medicine, Faculty of Medicine, Hiroshima University. We thank the Analysis Center of Life Science, Hiroshima University, for the use of their facilities. This work was supported in part by Grants-in-Aid for Cancer Research from the Ministry of Education, Culture, Science, Sports, and Technology of Japan.

Conflict of interest

None declared.

References

1 Rini BI, Campbell SC, Escudier B. Renal cell carcinoma. *Lancet* 2009; **373**: 1119–32.
2 Motzer RJ, Bander NH, Nanus DM. Renal-cell carcinoma. *N. Engl. J. Med.* 1996; **335**: 865–75.
3 Chow TF, Mankaruos M, Scorilas A *et al.* The miR-17-92 cluster is over expressed in and has an oncogenic effect on renal cell carcinoma. *J. Urol.* 2010; **183**: 743–51.
4 White NM, Bui A, Mejia-Guerrero S *et al.* Dysregulation of kallikrein-related peptidases in renal cell carcinoma: potential targets of miRNAs. *Biol. Chem.* 2010; **391**: 411–23.
5 Yousef GM. microRNAs: a new frontier in kallikrein research. *Biol. Chem.* 2008; **389**: 689–94.
6 Lu J, Getz G, Miska EA *et al.* MicroRNA expression profiles classify human cancers. *Nature* 2005; **435**: 834–8.
7 White NM, Bao TT, Grigull J *et al.* miRNA profiling for clear cell renal cell carcinoma: biomarker discovery and identification of potential controls and consequences of miRNA dysregulation. *J. Urol.* 2011; **186**: 1077–83.
8 Neal CS, Michael MZ, Rawlings LH, Van der Hoek MB, Gleadle JM. The VHL-dependent regulation of microRNAs in renal cancer. *BMC Med.* 2010; **8**: 1.
9 Petillo D, Kort EJ, Anema J, Furge KA, Yang XJ, Teh BT. MicroRNA profiling of human kidney cancer subtypes. *Int. J. Oncol.* 2009; **35**: 109–14.
10 Juan D, Alexe G, Antes T *et al.* Identification of a microRNA panel for clear cell kidney cancer. *Urology* 2010; **75**: 835–41.
11 Nakada C, Matsuura K, Tsukamoto Y *et al.* Genome-wide microRNA expression profiling in renal cell carcinoma: significant down-regulation of miR-141 and miR-200c. *J. Pathol.* 2008; **216**: 418–27.
12 Jung M, Mollenkopf HJ, Grimm C *et al.* MicroRNA profiling of clear cell renal cell cancer identifies a robust signature to define renal malignancy. *J. Cell. Mol. Med.* 2009; **13**: 3918–28.
13 Gottardo F, Liu CG, Ferracin M *et al.* Micro-RNA profiling in kidney and bladder cancers. *Urol. Oncol.* 2007; **25**: 387–92.
14 Yi Z, Fu Y, Zhao S, Zhang X, Ma C. Differential expression of miRNA patterns in renal cell carcinoma and nontumorous tissues. *J. Cancer Res. Clin. Oncol.* 2010; **136**: 855–62.
15 Chow TF, Youssef YM, Lianidou E *et al.* Differential expression profiling of microRNAs and their potential involvement in renal cell carcinoma pathogenesis. *Clin. Biochem.* 2010; **43**: 150–8.
16 Slaby O, Jancovicova J, Lakomy R *et al.* Expression of miRNA-106b in conventional renal cell carcinoma is a potential marker for prediction of early metastasis after nephrectomy. *J. Exp. Clin. Cancer Res.* 2010; **29**: 90.
17 Jiang S, Zhang HW, Lu MH *et al.* MicroRNA-155 functions as an OncomiR in breast cancer by targeting the suppressor of cytokine signaling 1 gene. *Cancer Res.* 2010; **70**: 3119–27.
18 Yanaihara N, Caplen N, Bowman E *et al.* Unique microRNA molecular profiles in lung cancer diagnosis and prognosis. *Cancer Cell* 2006; **9**: 189–98.
19 Greither T, Grochola L, Udelnow A, Lautenschläger C, Würl P, Taubert H. Elevated expression of microRNAs 155, 203, 210 and 222 in pancreatic tumors is associated with poorer survival. *Int. J. Cancer* 2010; **126**: 73–80.
20 Han ZB, Chen HY, Fan JW, Wu JY, Tang HM, Peng ZH. Up-regulation of microRNA-155 promotes cancer cell invasion and predicts poor survival of hepatocellular

carcinoma following liver transplantation. *J. Cancer Res. Clin. Oncol.* 2012; **138**: 153–61.
21 Shibuya H, Iinuma H, Shimada R, Horiuchi A, Watanabe T. Clinicopathological and prognostic value of microRNA-21 and microRNA-155 in colorectal cancer. *Oncology* 2010; **79**: 313–20.
22 Wotschofsky Z, Meyer HA, Jung M *et al.* Reference genes for the relative quantification of microRNAs in renal cell carcinomas and their metastases. *Anal. Biochem.* 2011; **417**: 233–41.
23 O'Connell RM, Chaudhuri AA, Rao DS, Baltimore D. Inositol phosphatase SHIP1 is a primary target of miR-155. *Proc. Natl. Acad. Sci. U.S.A.* 2009; **106**: 7113–18.
24 Gironella M, Seux M, Xie MJ *et al.* Tumor protein 53-induced nuclear protein 1 expression is repressed by miR-155, and its restoration inhibits pancreatic tumor development. *Proc. Natl. Acad. Sci. U.S.A.* 2007; **104**: 16170–5.
25 Harris AL. Hypoxia – a key regulatory factor in tumour growth. *Nat. Rev. Cancer* 2002; **2**: 38–47.
26 Bos R, van Diest PJ, de Jong JS, van der Groep P, van der Valk P, van der Wall E. Hypoxia-inducible factor-1alpha is associated with angiogenesis, and expression of bFGF, PDGF-BB, and EGFR in invasive breast cancer. *Histopathology* 2005; **46**: 31–6.
27 Bruning U, Cerone L, Neufeld Z *et al.* MicroRNA-155 promotes resolution of hypoxia-inducible factor-1α activity during prolonged hypoxia. *Mol. Cell. Biol.* 2011; **31**: 4087–96.
28 Lidgren A, Hedberg Y, Grankvist K, Rasmuson T, Bergh A, Ljungberg B. Hypoxia-inducible factor 1alpha expression in renal cell carcinoma analyzed by tissue microarray. *Eur. Urol.* 2006; **50**: 1272–7.
29 Moon EJ, Brizel DM, Chi JT, Dewhirst MW. The potential role of intrinsic hypoxia markers as prognostic variables in cancer. *Antioxid. Redox Signal.* 2007; **9**: 1237–94.
30 Schultz L, Chaux A, Albadine R *et al.* Immunoexpression status and prognostic value of mTOR and hypoxia-induced pathway members in primary and metastatic clear cell carcinomas. *Am. J. Surg. Pathol.* 2011; **35**: 1549–56.

Supporting information

Additional Supporting Information may be found in the online version of this article:

Fig. S1 (A) Expression of RNU48 between tumor and normal kidney tissue in 77 matched pairs of clear renal cell carcinoma samples ($P = 0.9896$). (B) Expression level of RNU48 in different sexes ($P = 0.6206$), sides ($P = 0.9654$), histological grades ($P = 0.9849$), infiltrating type ($P = 0.5084$), pT stages ($P = 0.8572$), pN stages ($P = 0.7671$), venous invasion ($P = 0.9540$), M stages ($P = 0.6206$) and stages ($P = 0.8576$) in 137 clear renal cell carcinoma samples. Whiskers depict the 5 and 95 percentiles.

Med Mol Morphol (2013) 46:20–23
DOI 10.1007/s00795-012-0004-x

ORIGINAL PAPER

Expression of podoplanin/D2-40 in pericryptal stromal cells in superficial colorectal epithelial neoplasia

Hirofumi Nakayama · Hideaki Enzan · Wataru Yasui

Received: 15 August 2011 / Accepted: 25 October 2011 / Published online: 10 January 2013

Abstract The aim of this study is to investigate the distribution and roles of podoplanin/D2-40-positive pericryptal stromal cells in superficial colorectal epithelial neoplasia. A total of 105 superficial colorectal epithelial tumors were examined: 65 tubular/tubulovillous adenomas, 32 adenocarcinomas in situ, and 8 submucosally invasive adenocarcinomas. Immunohistochemical analysis was performed using the monoclonal antibody to podoplanin/clone D2-40, which is reactive in both lymphatic endothelial cells and activated stromal cells, but negative in vascular endothelial cells. We found 50 (78 %) of 65 tubular/tubulovillous adenomas, 30 (94 %) of 32 adenocarcinomas in situ, and all 8 (100 %) submucosally invasive adenocarcinomas had podoplanin/D2-40-positive pericryptal stromal cells, whereas all normal colorectal mucosae had no podoplanin/D2-40-positive pericryptal stromal cells. The presence of podoplanin/D2-40-positive pericryptal stromal cells is associated with epithelial tumorigenesis in the colorectum.

All of this paper was presented at the 24th Annual Meeting of the Japanese Society for Clinical Molecular Morphology.

H. Nakayama (✉)
Department of Pathology and Laboratory Medicine,
Hiroshima General Hospital of West Japan Railway Company,
3-1-36 Futabanosato, Higashi-ku,
Hiroshima 732-0057, Japan
e-mail: hinakayama-path@umin.ac.jp

H. Enzan
Department of Diagnostic Pathology,
Chikamori Hospital, Kochi, Japan

W. Yasui
Department of Molecular Pathology,
Institute of Biomedical and Health Sciences,
Hiroshima University, Hiroshima, Japan

Keywords Podoplanin · D2-40 · Colorectum · Adenoma · Adenocarcinoma

Introduction

A monoclonal antibody clone D2-40, originally raised against an unidentified M2A protein derived from germ cell tumors [1], specifically recognizes podoplanin [2]. D2-40 is reactive in lymphatic endothelial cells, but not in vascular endothelial cells [3]. Therefore, D2-40 is a useful immunohistochemical marker for discriminating invasion of lymphatic vessels from that of capillaries, venules, and veins in paraffin sections of primary tumors including cancers of breast, colon, prostate, cervix, endometrium, and skin (melanomas and squamous cell carcinomas) [4]. Podoplanin is also detected in type I alveolar cells, glomerular podocytes, bile duct cells, peritoneal mesothelial cells, osteocytes, periosteal cells, myoepithelial cells of breast and salivary glands, choroid plexus, ependymal cells, meninges, basal keratinocytes of skin, esophagus and uterine cervix, and stromal reticular cells and follicular dendritic cells of lymphoid organs [2].

More recently, podoplanin is also identified in cancer stromal fibroblasts, which is a favorable prognostic marker in patients with colorectal carcinomas [5] and uterine cervical carcinomas [6], but is a poor prognosis of lung adenocarcinomas [7, 8]. No research has been performed regarding gastrointestinal superficial tumors and tumor-like lesions.

To investigate a relationship between colorectal epithelial tumorigenesis and the presence of podoplanin/D2-40-positive pericryptal stromal cells, immunostaining for podoplanin/D2-40 was performed in colorectal adenoma, adenocarcinoma in situ, and submucosally invasive adenocarcinoma.

Materials and methods

We examined 105 endoscopically resected superficial colorectal tumors and tumor-like lesions (65 tubular/tubulovillous adenomas, 32 adenocarcinomas in situ, and 8 submucosally invasive adenocarcinomas) and their paired normal mucosae; all the cases were diagnosed by the authors (H.N. and W.Y.). Regarding sessile serrated adenomas/polyps and traditional serrated adenomas, it is still controversial to apply the proposed criteria [9] to practical diagnostic pathology. Thus, we excluded these serrated lesions. Specimens were fixed in 10 % formalin, embedded in paraffin, and cut into sections 4 μm thick for hematoxylin and eosin (H&E) staining and immunohistochemistry. The maximum tumor cut surface was immunostained in all the tumors examined.

Immunohistochemical studies were performed by the labeled streptavidin–biotin method using a Dako kit (Dako Japan, Kyoto), and the mouse monoclonal antibodies against podoplanin (clone D2-40; Nichirei, Tokyo, Japan, 1:50) were used. Before incubation with the primary antibody, the sections were microwaved for 40 min in citrate buffer (pH 6.0).

We regarded a single row of podoplanin/D2-40-positive stromal cells immediately facing glands to be podoplanin/D2-40-positive pericryptal stromal cells. Desmoplastic stromal cells are spindle cells having vesicular nuclei and pale eosinophilic cytoplasm and forming bundles located between carcinoma glands [10]. Neither quantitative nor semiquantitative analysis was performed.

Results

Table 1 summarizes the results.

In all normal colorectal mucosa, no podoplanin/D2-40-positive pericryptal stromal cells were seen (Fig. 1).

In contrast, 50 (78 %) of 65 tubular/tubulovillous adenomas and 30 (94 %) of 32 adenocarcinomas in situ had a single row of podoplanin/D2-40-positive pericryptal stromal cells (Figs. 2, 3).

In all eight submucosally invasive adenocarcinomas, podoplanin/D2-40 was positive in desmoplastic stromal cell bundles (Fig. 4).

Discussion

Desmoplastic cancer stromal cells in various organs are positive for podoplanin/D2-40; presence of podoplanin/D2-40-positive desmoplastic stromal cells is associated with prognosis of human cancers [5–8]. The presence of podoplanin/D2-40-positive desmoplastic stromal cells is related

Table 1 Podoplanin/D2-40-positive stromal cells in superficial colorectal epithelial neoplasia

Histological type	Number of lesions	D2-40(+) cells	
		Pericryptal periglandular	Desmoplastic stromal cell bundles
Normal colorectal crypts	105	0	–
Tubular/tubulovillous			
Adenomas	65	50 (78 %)	–
Adenocarcinomas in situ	32	30 (94 %)	–
Submucosally invasive adenocarcinomas	8	0	8 (100 %)

Fig. 1 Normal colorectal crypts. No podoplanin/D2-40-positive pericryptal stromal cells are detected. ×200

Fig. 2 Tubular adenoma. Podoplanin/D2-40-positive stromal cells are seen facing the crypts. ×200

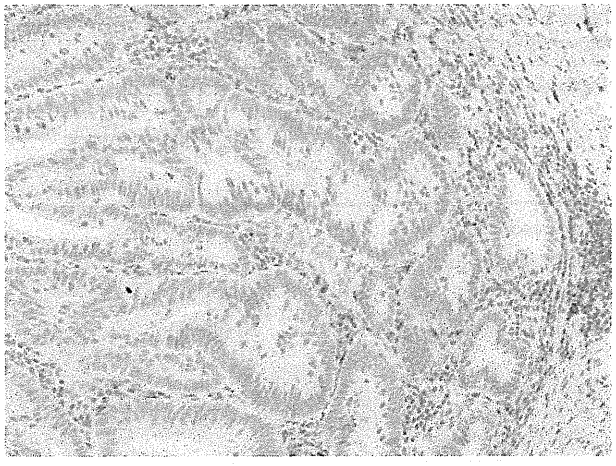

Fig. 3 Adenocarcinoma in situ. Podoplanin/D2-40-positive stromal cells are observed facing the crypts. ×200

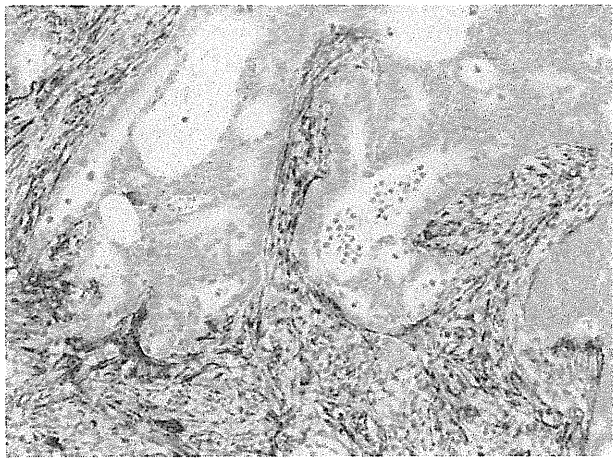

Fig. 4 Invasive adenocarcinoma. Podoplanin/D2-40 is positive in desmoplastic stromal cells. ×200

to a favorable prognosis of colorectal adenocarcinomas [5] and uterine cervical squamous cell carcinomas [6], but to a poor prognosis of lung adenocarcinomas [7, 8]. In intrahepatic cholangiocarcinomas, the presence of podoplanin/D2-40-positive myofibroblasts is related to lymphatic spread [11]. Podoplanin/D2-40 is also known as an immunohistochemical marker for myoepithelial cells of breast and the precaution in interpreting tumor lymphovascular invasion of breast cancer [12]. Podoplanin/D2-40 is also proposed as a novel immunohistochemical marker in differentiating dermatofibroma from dermatofibrosarcoma protuberans; all dermatofibromas examined demonstrate strong and diffuse immunoreactivity to podoplanin/D2-40, whereas no dermatofibrosarcomas protuberans were labeled by podoplanin/D2-40 [13]. However, there have been no reports from the point of view of molecular morphology in gastrointestinal epithelial tumorigenesis.

In the present study, no podoplanin/D2-40-positive pericryptal stromal cells were seen in normal colorectal mucosa, whereas a single row of podoplanin/D2-40-positive pericryptal stromal cells was present in adenomas and adenocarcinomas in situ. In submucosally invasive adenocarcinomas, neoplastic glands were not surrounded by a single row of podoplanin/D2-40-positive periglandular stromal cells; podoplanin/D2-40 was positive in the desmoplastic stromal cell bundles. Superficial colorectal epithelial tumors with podoplanin/D2-40-positive stromal cell bundles are submucosally invasive carcinomas. In the colorectum, podoplanin/D2-40 immunostaining is helpful for differentiating adenomas and adenocarcinomas in situ from submucosally invasive adenocarcinomas. Pericryptal fibroblasts (PCFs) exist in normal colorectal mucosa [14]. PCFs express not only alpha-smooth muscle actin, but also high molecular weight caldesmon, highly specific for smooth muscle cells [15]. PCFs also exist in hyperplastic polyps and adenomas but not in invasive adeocarcinomas [16, 17]. Thus, the present results suggest that the podoplanin/D2-40-positive pericryptal stromal cells are podoplanin/D2-40-positive PCFs. To elucidate the relationship between colorectal PCFs in normal colorectal mucosa and podoplanin/D2-40-positive pericryptal stromal cells, further comprehensive studies that include double staining with other markers such as alpha-smooth muscle actin [10], Prox 1 [18] and CD31 [19] should be performed.

The presence of podoplanin/D2-40-positive pericryptal stromal cells is associated with epithelial tumorigenesis in the colorectum. Podoplanin could have a supportive role in colorectal epithelial tumorigenesis. To elucidate whether podoplanin expression in pericryptal stromal cells is a consequence or a cause of colorectal adenoma and adenocarcinoma in situ, both comprehensive cell biological and in vivo studies should be performed, by using podoplanin knockout mice, cultured PCFs, and antisense oligonucleotide targeting podoplanin.

Acknowledgments The authors are grateful to all the medical technologists in the Pathology Division, Hiroshima City Medical Association Clinical Laboratory, for their excellent technical assistance.

References

1. Marks A, Sutherland DR, Bailey D, Iglesias J, Law J, Lei M, Yeger H, Banerjee D, Baumal R (1999) Characterization and distribution of an oncofetal antigen (M2A antigen) expressed on testicular germ cell tumors. Br J Cancer 80:569–578
2. Schacht V, Dadras SS, Johnson LA, Jackson DG, Hong YK, Detmar M (2005) Up-regulation of the lymphatic marker podoplanin, a mucin-type transmembrane glycoprotein, in human squamous cell carcinomas and germ cell tumors. Am J Pathol 166:913–921

3. Kahn HJ, Bailey D, Marks A (2002) Monoclonal antibody D2–40, a new marker of lymphatic endothelium, reacts with Kaposi's sarcoma and a subset of angiosarcomas. Mod Pathol 15:434–440
4. Kahn HJ, Marks A (2002) A new monoclonal antibody, D2–40, for detection of lymphatic invasion in primary tumors. Lab Invest 82:1255–1257
5. Yamanashi T, Nakanishi Y, Fujii G, Akishima-Fukasawa Y, Moriya Y, Kanai Y, Watanabe M, Hirohashi S (2009) Podoplanin expression identified in stromal fibroblasts as a favorable prognostic marker in patients with colorectal carcinoma. Oncology 77:53–62
6. Carvalho FM, Zaganelli FL, Almeida BG, Goes JC, Baracat EC, Carvalho JP (2010) Prognostic value of podoplanin expression in intratumoral stroma and neoplastic cells of uterine cervical carcinomas. Clinics (Sao Paulo) 65:1279–1283
7. Kitano H, Kageyama S, Hewitt SM, Hayashi R, Doki Y, Ozaki Y, Fujino S, Takikita M, Kubo H, Fukuoka J (2010) Podoplanin expression in cancerous stroma induces lymphangiogenesis and predicts lymphatic spread and patient survival. Arch Pathol Lab Med 134:1520–1527
8. Kawase A, Ishii G, Nagai K, Ito T, Nagano T, Murata Y, Hishida T, Nishimura M, Yoshida J, Suzuki K, Ochiai A (2008) Podoplanin expression by cancer associated fibroblasts predicts poor prognosis of lung adenocarcinoma. Int J Cancer 123:1053–1059
9. Snover DC, Ahnen DJ, Burt RW, Odze RD (2010) Serrated polyps of the colon and rectum and serrated polyposis. In: Bosman FT, Carneiro F, Hruban RH et al (eds) WHO classification of tumors of the digestive system, 4th edn. IARC, Lyon, pp 160–165
10. Nakayama H, Enzan H, Miyazaki E, Naruse K, Kiyoku H, Hiroi M (1998) The role of myofibroblasts at the tumor border of invasive colorectal adenocarcinomas. Jpn J Clin Oncol 28: 615–620
11. Aishima S, Nishihara Y, Iguchi T, Taguchi K, Taketomi A, Maehara Y, Tsuneyoshi M (2008) Lymphatic spread is related to VEGF-C expression and D2–40-positive myofibroblasts in intrahepatic cholangiocarcinoma. Mod Pathol 21:256–264
12. Ren S, Abel-Haija M, Khurana JS, Zhang X (2011) D2-40: an additional marker for myoepithelial cells of breast and the precaution in interpreting tumor lymphovascular invasion. Int J Clin Exp Pathol 4:175–182
13. Bandarchi B, Ma L, Marginean C, Hafezi S, Zubovits J, Rasty G (2010) D2-40, a novel immunohistochemical marker in differentiating dermatofibroma from dermatofibrosarcoma protuberans. Mod Pathol 23:434–438
14. Sappino AP, Dietrich PY, Skalli O, Widgren S, Gabbiani G (1989) Colonic pericryptal fibroblasts. Differentiation pattern in embryogenesis and phenotypic modulation in epithelial proliferative lesions. Virchows Arch A Pathol Anat Histopathol 415:551–557
15. Nakayama H, Miyazaki E, Enzan H (1999) Differential expression of high molecular weight caldesmon in colorectal pericryptal fibroblasts and tumor stroma. J Clin Pathol 52:785–786
16. Yao T, Tsuneyoshi M (1993) Significance of pericryptal fibroblasts in colorectal epithelial tumors: a special reference to the histologic features and growth patterns. Hum Pathol 24:525–533
17. Adegboyega PA, Mifflin RC, DiMari JF, Saada JI, Powell DW (2002) Immunohistochemical study of myofibroblasts in normal colonic mucosa, hyperplastic polyps, and adenomatous colorectal polyps. Arch Pathol Lab Med 126:829–836
18. Wigle JT, Oliver G (1999) Prox1 function is required for the development of the murine lymphatic system. Cell 98:769–778
19. Miettinen M, Lindenmayer AE, Chaubal A (1994) Endothelial cell markers CD31, CD34, and BNH9 antibody to H-and Y-antigens: evaluation of their specificity and sensitivity in the diagnosis of vascular tumors and comparison with von Willebrand factor. Mod Pathol 7:82–90

Gastric Cancer (2013) 16:345–354
DOI 10.1007/s10120-012-0191-0

ORIGINAL ARTICLE

Decreased FANCJ caused by 5FU contributes to the increased sensitivity to oxaliplatin in gastric cancer cells

Ryutaro Mori · Kazuhiro Yoshida · Toshiyuki Tanahashi · Kazunori Yawata · Junko Kato · Naoki Okumura · Yasuhiro Tsutani · Morihito Okada · Naohide Oue · Wataru Yasui

Received: 13 January 2012 / Accepted: 13 August 2012 / Published online: 12 September 2012

Abstract
Background Oxaliplatin is effective against many types of cancer, and the combination of 5-fluorouracil (5FU) and oxaliplatin is synergistically effective against gastric cancer, as well as colon cancer. The FANCJ protein is one of the Fanconi anemia (FA) gene products, and its interaction with the tumor suppressor BRCA1 is required for DNA double-strand break (DSB) repair. FANCJ also functions in interstrand crosslinks (ICLs) repair by linking to mismatch repair protein complex MLH1-PMS2 (MutLα). While oxaliplatin causes ICLs, 5FU is considered to cause DSBs. Therefore, we investigated the importance of FANCJ in the synergistic effects of oxaliplatin and 5FU in MKN45 gastric cancer cells and the derived 5FU-resistant cell line, MKN45/F2R.
Methods MKN1, TMK1, MKN45, and MKN45/F2R (5FU-resistant) gastric cancer cells were treated with 5FU and/or oxaliplatin. The signaling pathway was evaluated by a western blotting analysis and reverse transcription polymerase chain reaction (RT-PCR). Drug resistance was evaluated by the 3-(4,5-dimethyl-2-tetrazolyl)-2,5-diphenyl-2H tetrazolium bromide (MTT) assay.
Results In MKN45 cells, the combination of 5FU and oxaliplatin had synergistic effects. DSBs appeared when the cells were treated with 5FU. FANCJ was down-regulated, and BRCA1 was induced in a dose- and time-dependent manner. MKN45 cells showed increased sensitivity to oxaliplatin when FANCJ was knocked down by short interfering (si) RNA. However, these findings were not observed in MKN45/F2R 5FU-resistant cells.
Conclusion These results strongly suggest that the decrease in FANCJ caused by 5FU treatment leads to an increase in sensitivity to oxaliplatin, thus indicating that the FANCJ protein plays an important role in the synergism of the combination of 5FU and oxaliplatin.

Keywords Fluorouracil · Oxaliplatin · BACH1 protein

R. Mori · K. Yoshida (✉) · T. Tanahashi · K. Yawata · J. Kato · N. Okumura
Department of Surgical Oncology, Gifu University, Graduate School of Medicine, 1-1 Yanagido, Gifu, Gifu 501-1194, Japan
e-mail: kyoshida@gifu-u.ac.jp

Y. Tsutani · M. Okada
Department of Surgical Oncology, Research Institute for Radiation Biology and Medicine, Hiroshima University, Hiroshima, Japan

N. Oue · W. Yasui
Department of Molecular Pathology, Hiroshima University Graduate School of Medicine, Hiroshima, Japan

Introduction

Gastric cancer remains one of the major causes of cancer deaths around the world [1, 2]. Most patients with advanced and metastatic gastric cancer are treated with chemotherapy, and the combination of S-1 and cisplatin (CDDP) is one of the standard first-line regimens used in Japan [3].

The combination of fluorouracil (5FU) and oxaliplatin is used in the fluorouracil, leucovorin, and oxaliplatin (FOLFOX) regimen for colorectal cancer, and its efficacy has been clinically confirmed [4]. Oxaliplatin exerts growth inhibitory effects on many cancer cell lines and tumors, including some that are primarily resistant to CDDP and carboplatin. This increased activity is due to its 1, 2-diaminocyclohexane (DACH) carrier ligand, which provides higher lipophilicity, as evidenced by its large volume of distribution and slow excretion through the kidneys [5]. The combination of 5FU and oxaliplatin against gastric cancer

has been demonstrated to be effective in the clinic [6, 7], and oxaliplatin is sometimes used to replace CDDP for the treatment of gastric cancer, because of its better tolerability [8]. Oxaliplatin and 5FU have demonstrated activity against colon cancer cell lines, and synergistic activity between the agents has been observed in experimental models [9, 10], but the mechanism underlying their synergistic effect is unclear.

The FANCJ protein is one of the Fanconi anemia (FA) gene products. It was first identified as a protein that binds directly to the breast cancer-associated tumor suppressor, BRCA1 [11, 12], and was originally named BACH1/BRIP1 [12, 13]. Fanconi anemia is a rare hereditary disorder characterized by skeletal abnormalities, bone marrow failure, and an increased incidence of cancer. The basic cellular abnormality in FA has been postulated to lie in the DNA repair mechanisms, because cells from FA patients display chromosomal abnormalities and are hypersensitive to agents that cause DNA interstrand crosslinks (ICLs), such as mitomycin C (MMC) and CDDP [14]. The role of FANCJ in the FA pathway has not yet been completely elucidated. So far, it has been shown that FANCJ is a DNA helicase for the D-loop structure in the early stage of the homologous recombination (HR) pathway of double-strand break (DSB) repair; therefore, the association of FANCJ with BRCA1 is essential for DSB repair [12, 13]. Moreover, FANCJ interacts with the mismatch repair complex MutLα, composed of MLH1 and PMS2, independent of BRCA1, and the FANCJ/MutLα interaction is essential for ICL repair [15].

It is known that 5FU induces DSBs as a result of its incorporation into DNA [16] or thimidylate synthase (TS) inhibition [17], and oxaliplatin induces ICLs by its pharmacological action. Based on these facts, we hypothesized that the two functions of FANCJ would be involved in the synergistic effects of 5FU and oxaliplatin against gastric cancer.

In the present study, we clarified the differential regulation of the FANCJ protein between 5FU-sensitive and 5FU-resistant cells and also demonstrated the mechanism underlying the synergistic effects of 5FU and oxaliplatin against gastric cancer cells.

Materials and methods

Drugs

5FU was purchased from Kyowa Hakko (Tokyo, Japan), and oxaliplatin was purchased from Yakult Honsha (Tokyo, Japan).

Cell lines and cell culture

Gastric cancer cell lines (MKN45, MKN1, TMK1) were cultured in RPMI 1640 medium (Wako, Osaka, Japan) supplemented with 10 % fetal bovine serum (Sigma-Aldrich, St. Louis, MO, USA), antibiotics (Sigma-Aldrich), and HEPES (Sigma-Aldrich) in a humidified atmosphere of 5 % CO_2 at 37 °C. MKN45 and TMK1 are poorly differentiated human gastric adenocarcinoma cell lines. MKN1 is an adenosquamous carcinoma cell line. MKN45/F2R is a 5FU-resistant cell line. To establish this cell line, the MKN45 parent cells were continuously exposed to increasing concentrations (0.1–2 μM) of 5FU over a period of 1 year. The MKN45/F2R cells were routinely maintained in culture medium containing 2 μM of 5FU. To eliminate the effects of 5FU in our experiments, the resistant cells were cultured in a drug-free medium for at least 2 weeks before all of the studies [18].

3-(4,5-Dimethyl-2-tetrazolyl)-2,5-diphenyl-2H tetrazolium bromide (MTT) assay for the effects of 5FU or oxaliplatin on cell viability

Cell growth was assessed with a standard MTT assay, which detects the dehydrogenase activity in viable cells. A total of 5×10^3 cells were seeded in each well of 96-well culture plates. After 24 h, the cells were treated with various concentrations of drugs. After another 72 h, the culture medium was removed, and 100 μl of a 0.5 mg/ml solution of MTT (Sigma-Aldrich) was added to each well. The plates were then incubated for 4 h at 37 °C. The MTT solution was then removed and replaced with 100 μl of dimethyl sulfoxide (Wako) per well, and the absorbance at 540 nm was measured using an Envision 2104 Multilabel Reader (Perkin Elmer, Waltham, MA, USA).

The Combination Index (CI) was calculated by the formula $CI = A/Ax + B/Bx$ (A: the 50% inhibitory concentration [IC50] for drug A in combination, Ax: the IC50 for drug A alone, B: the IC50 for drug B in combination, Bx: the IC50 for drug B alone) (based on the Loewe additivity model [19]).

Immunofluorescence for γH2AX

The cells were harvested in a Lab-Tek Chamber Slide System (Thermo Fisher Scientific, Waltham, MA, USA) and immunofluorescence studies were performed. The cells were first fixed in 4 % paraformaldehyde for 15 min at room temperature and washed three times with phosphate-buffered saline (PBS) containing 1 % Triton X-100 (PBST). Blocking against non-specific binding was performed for 60 min with 0.5 % goat serum dissolved in PBST, and the cells were again washed three times with PBST. The rabbit monoclonal anti-phospho-H2AX antibody (Cell Signaling Technology, Danvers, MA, USA, 1:200) was used as the primary antibody. The cells were incubated for 1 h at room temperature with the primary antibody dissolved in PBST

supplemented with 0.5 % goat serum, and then the cells were washed three more times with PBST. The cells were then incubated with highly cross-adsorbed Alexa Fluor 546 goat anti-rabbit IgG (Invitrogen, Carlsbad, CA, USA, 4 μg/ml), Phalloidin Alexa Fluor 488 Conjugate (Lonza, Walkersville, MD, USA, 1:40), and 4', 6-diamidino-2-phenylindole (DAPI) Nucleic Acid Stain (Invitrogen 1:25000) in PBST containing 0.5 % goat serum. Images were acquired on a DP70-WPC02 camera mounted on an IX50 system (Olympus, Tokyo, Japan).

Immunoprecipitation, western blot analysis, and antibodies

Cells were harvested and lysed in CelLytic™ M (Sigma-Aldrich) for 30 min on ice. The protein concentration of the lysates was measured using a DC Protein Assay Kit (Bio-Rad, Hercules, CA, USA). For the immunoprecipitation assays, cell lysates were incubated with an anti-FANCJ antibody (Abcam, Cambridge, UK, 1:100) for 2 h at 4 °C and PureProteome™ Protein A Magnetic Beads (Millipore, Billerica, MA, USA) were added, and the beads were subsequently washed. The cell lysates were boiled in Sample Buffer Solution (Wako), then total cell protein extracts (20 μg/lane) were separated by sodium dodecyl sulfate–polyacrylamide gel electrophoresis using SuperSep™ (Wako), and they were electrophoretically transferred onto polyvinyl difluoride (PVDF) membranes. The membranes were blocked with PVDF blocking reagent (TOYOBO, Osaka, Japan) for 1 h. The membranes were then incubated with primary antibodies against β-actin, FANCJ, BRCA1, FANCD1/BRCA2, phospho-Histone H2AX(Ser139) (Cell Signaling Technology, 1:5000), MLH1 (Abcam, 1:100000), FANCD2 (Abcam, 1:50000), and PMS2 (EPITOMICS, San Francisco, CA, USA, 1:20000) overnight at 4 °C. The primary antibodies were diluted with Can Get Signal Solution 1 (TOYOBO). The membranes were then washed with Dako Washing Buffer (Dako, Glostrup, Denmark) and incubated with the appropriate secondary antibodies (Millipore, 1:25000). Secondary antibodies were diluted with Can Get Signal Solution 2 (TOYOBO). The immunoreactive proteins were visualized by chemiluminescence using ImmunoStar LD reagents (Wako), and images were captured by an LAS-4000 system (FUJIFILM, Tokyo, Japan).

Transfection and small interfering RNA experiments for FANCJ

The MKN45 cells were cultured in medium without antibiotics for 24 h before transfection at 50–70 % confluence. The cells were transfected with a small interfering RNA (siRNA) oligonucleotide using Lipofectamine RNAiMAX (Invitrogen) in a final siRNA concentration of 40 nmol/l in serum-free Opti-MEM (Invitrogen). After 48 h, the total RNA and proteins were extracted, and the expression levels of the FANCJ mRNA and protein were analyzed by real-time reverse transcription polymerase chain reaction (RT-PCR) and a western blotting analysis, respectively. The siRNA oligonucleotides (Stealth RNAi) and the negative control oligonucleotides (Stealth RNAi siRNA Negative Control) for FANCJ were purchased from Invitrogen.

Results

The combination of 5FU and oxaliplatin has synergistic effects against MKN45 cells

To verify that there were synergistic effects of 5FU and oxaliplatin against gastric cancer cells, we performed the MTT assay using 5FU and oxaliplatin in MKN1, TMK1, MKN45, and MKN45/F2R (5FU-resistant) cells (Fig. 1a–d), and calculated the IC50 and the CI using the Loewe additivity model [19] (Table 1). The MKN45/F2R cells were previously established as 5FU-resistant cells in our laboratory [18]. The IC50 of MKN45/F2R cells for 5FU in the present study was 52.4 μM, which is 46.0-fold increased resistance compared with the parent MKN45 cell line, for which the IC50 of 5FU was 1.14 μM, while the major characteristics of these cell lines were consistent, as reported previously [18]. In the MKN45 cells, when 0.1 μM of 5FU was combined with oxaliplatin, the CI was 0.439, which was significantly lower than 1 ($p < 0.05$). This means that the combination had a synergistic effect. Conversely, no synergistic effect was observed in the MKN1, TMK1, and MKN45/F2R cells.

Changes in ICL repair proteins after 5FU treatment

Oxaliplatin induces its cytotoxic effects primarily by inducing ICLs. We herein examined the differential expression of the proteins involved in ICL repair by a western blotting analysis after treating MKN45 gastric cancer cells with 1 μM, 10 μM, or 100 M of 5FU for 24 h. The proteins examined included FANCJ, BRCA1, MLH1, PMS2, FANCD2, and FANCD1/BRCA2. The FANCJ protein, which is one of the FA gene products, and the tumor suppressor BRCA1 are required to repair DSBs [12, 13]. FANCJ also functions in ICL repair by linking to mismatch repair protein complex MLH1-PMS2 (MutLα) [15]. FANCD1/BRCA2 and FANCD2 are the key proteins in the FA pathway [14]. Interestingly, we observed that the expression of the FANCJ protein was decreased in a dose-dependent manner, and the expression was decreased to 48 % at 100 μM of 5FU compared to the expression level without 5FU. On the other hand, the expression of the

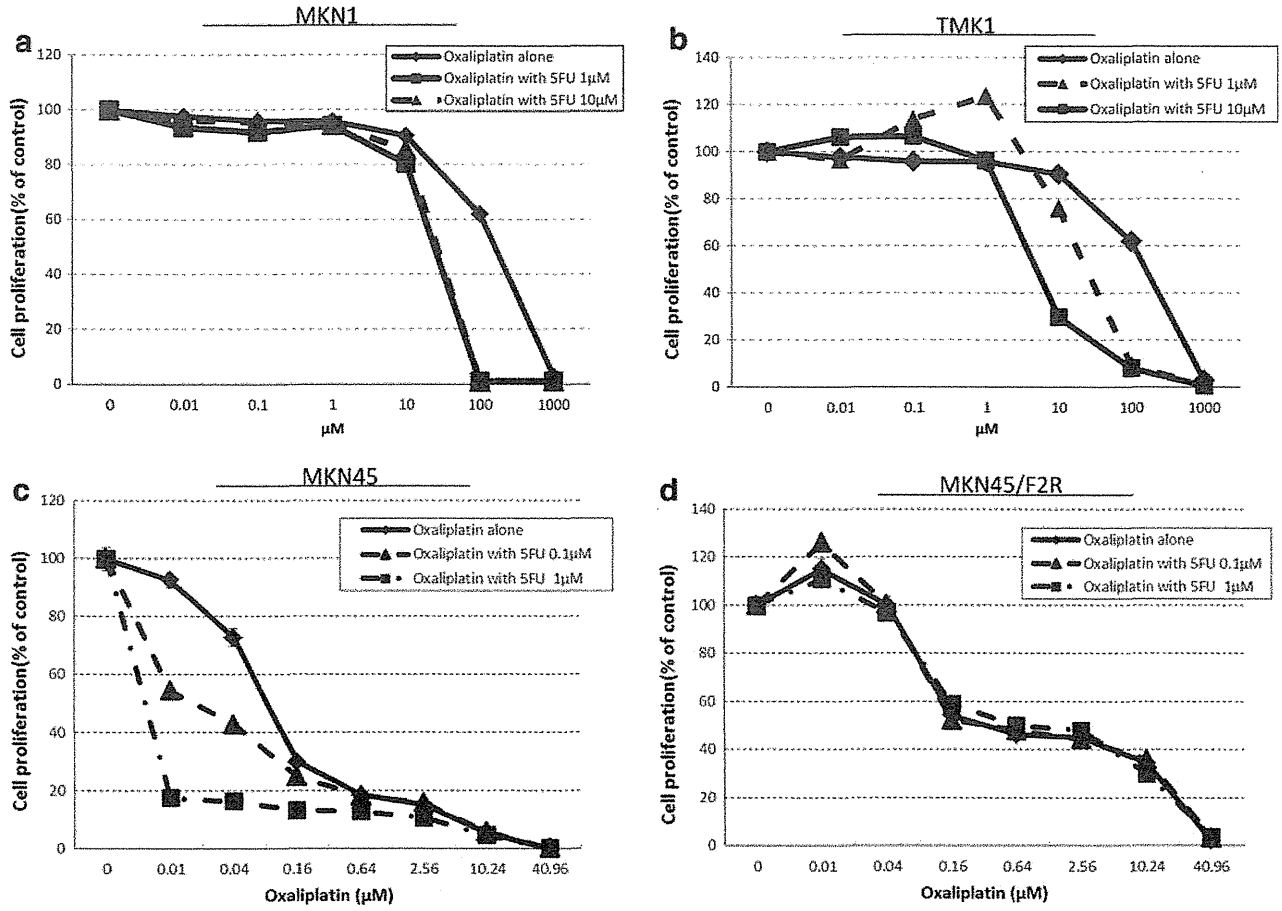

Fig. 1 The in vitro sensitivity of the MKN1, TMK1, MKN45 and MKN45/F2R cells to oxaliplatin and/or 5-fluorouracil (*5FU*). **a**, **b**, **d** No synergistic effect was observed at any concentration of 5FU in the MKN1, TMK1, and MKN45/F2R cells. **c** In the MKN45 cells, when 5FU was combined with oxaliplatin, a synergistic effect was observed

Table 1 IC50 values for 5FU and/or oxaliplatin in gastric cancer cells

Drug	MKN1	TMKN1	MKN45	MKN45-F2R
5FU alone	205.50 ± 4.62	297.89 ± 8.92	1.14 ± 0.888	52.4 ± 8.35
Oxaliplatin alone	159.65 ± 4.21	400.66 ± 8.32	0.177 ± 0.00992	2.58 ± 0.311
Oxaliplatin with 0.1 μM 5FU	24.116 ± 0.3425	25.539 ± 1.6378	0.0877 ± 0.00126*	0.317 ± 0.474
Oxaliplatin with 1 μM 5FU	26.315 ± 0.5236	4.99 ± 0.4615	–	0.61 ± 0.526

The 50% inhibitory concentration (IC50) values were calculated from the results of the MTT assay for oxaliplatin and/or 5-fluorouracil (5FU) in the MKN1, TMK1, MKN45, and MKN45/F2R cells. The combination index (CI) was calculated using the Loewe additivity model [19], and a synergistic effect was observed when 0.1 μM of 5FU was combined with oxaliplatin in MKN45 cells (CI = 0.439 ± 0.077**). The IC50 value could not be calculated for these cells when 1 μM of 5FU was combined with oxaliplatin, because the IC50 value was lower than the lowest concentration used in this experiment

* $p < 0.05$ based on Student's *t*-test

** $p < 0.05$ based on Student's *t*-test compared to 1

BRCA1 protein was increased by 2.1-fold after treatment with 1 μM of 5FU. These changes indicated that FANCJ and BRCA1 functioned to repair the DSBs caused by 5FU, and these proteins were likely to be related to the synergism between 5FU and oxaliplatin, because a deficit of FANCJ protein leads to a failure of ICL repair [15]. None of the expression levels of other proteins involved in DSB or ICL repair, such as MutLα, were changed, or they were only slightly increased after 5FU treatment, and seemed not to be involved in the synergism between 5FU and oxaliplatin.

We also examined the expressions of FANCJ and BRCA1 in other gastric cancer cell lines, such as MKN1,

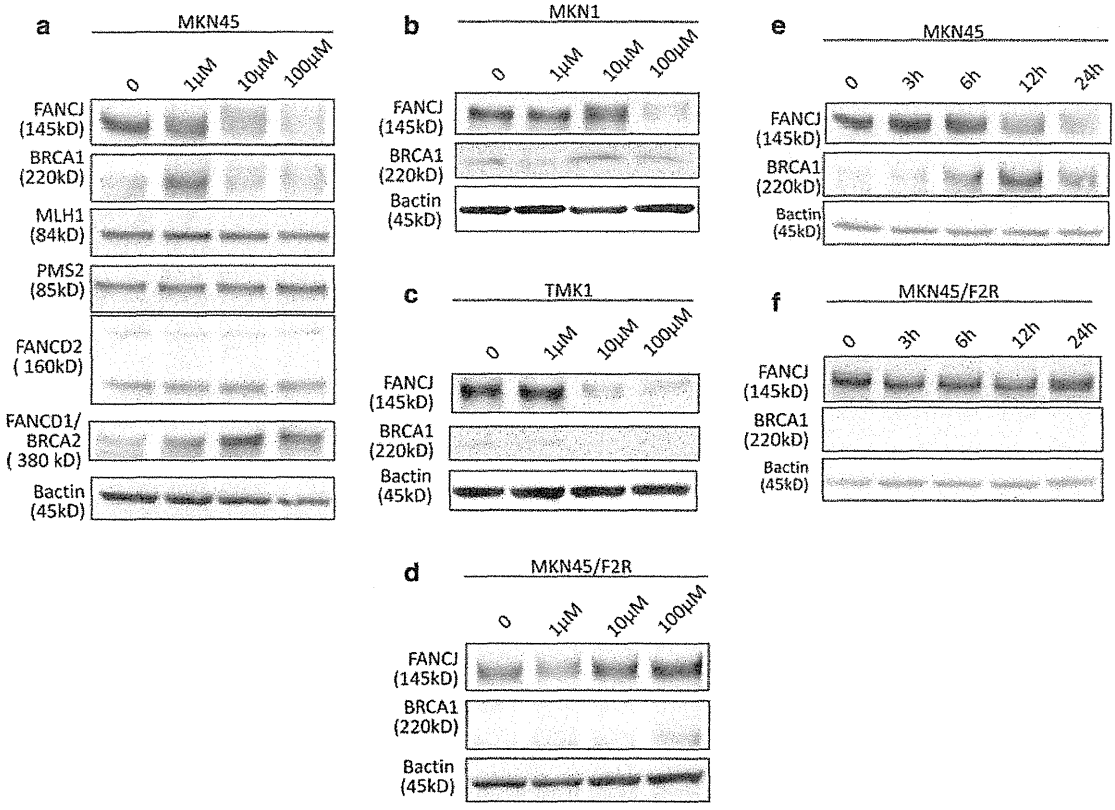

Fig. 2 Changes in interstrand crosslink (ICL) repair proteins after 5FU treatment. **a** The results of a western blotting analysis of the expression of FANCJ, BRCA1, MLH1, PMS2, FANCD2, and FANCD1/BRCA2 in MKN45 cells treated with 5FU at 1, 10, and 100 μM for 24 h. **b** The results of the western blotting analysis of FANCJ and BRCA1 in MKN1 cells. **c** The results of the western blotting analysis in TMK1 cells. **d** The results of the western blotting analysis in MKN45/F2R cells. **e** The results of the western blotting analysis of the expression of FANCJ and BRCA1 in MKN45 cells treated with 10 μM of 5FU for 3, 6, 12, and 24 h. **f** The results of the western blotting analysis of the expression of these proteins in MKN45/F2R cells treated with 10 μM of 5FU for 3, 6, 12, and 24 h

TMK1, and MKN45/F2R cells. As shown in Fig. 2b–d. The downregulation of FANCJ was reproduced in MKN1 and TMK1 cells, and induction of BRCA1 was also observed in MKN1 cells. In the MKN45/F2R cells, both FANCJ and BRCA1 were unchanged after 5FU treatment.

We then treated MKN45 and MKN45/F2R cells with 10 μM of 5 FU for 3, 6, 12, and 24 h and examined the FANCJ and BRCA1 expression levels by a western blot analysis; as shown in Fig. 2e, f the FANCJ expression in the MKN45 parental cells was decreased and BRCA1 expression was increased in a time-dependent manner. The FANCJ protein was decreased to 48 % of the level of the control after a 24-h treatment, while the expression of BRCA1 was increased by 4.3-fold compared to the control level. These changes were not observed in MKN45/F2R cells.

DSBs appeared when MKN45 cells were treated with 5FU

It has previously been established that 5FU induces DSBs, and FANCJ functions in DSB repair [12, 13]. Therefore, we examined whether DSBs occurred in MKN45 and MKN45/F2R cells treated with 5FU.

To evaluate the DSB status, we performed immunofluorescence studies for γH2AX, which is a marker of DSBs [20, 21]. There were indeed DSBs, which are indicated in red in Fig. 3a. The MKN45 and MKN45/F2R cells were treated with 5FU at concentrations of 1, 10, and 100 μM for 24 h, and we found that DSBs were increased in a dose-dependent manner in the MKN45 parental cells, while this phenomenon was not observed in MKN45/F2R cells (Fig. 3a). We also treated the cells with 10 μM of 5FU for 3, 12, and 24 h, and examined the DSBs (Fig. 3b). As expected, the DSBs were observed in MKN45 parental cells, and they were increased in a time-dependent manner, with DSBs being present in 62 % of the cells after the 24-h treatment. However, no time-dependent DSBs were detected in the MKN45/F2R cells.

Next, we performed a Western blot analysis for γH2AX after 5FU treatment to confirm the increased expression of the protein. The expression of γH2AX was increased by 6.2-fold after treatment with 10 and 100 μM of 5FU for

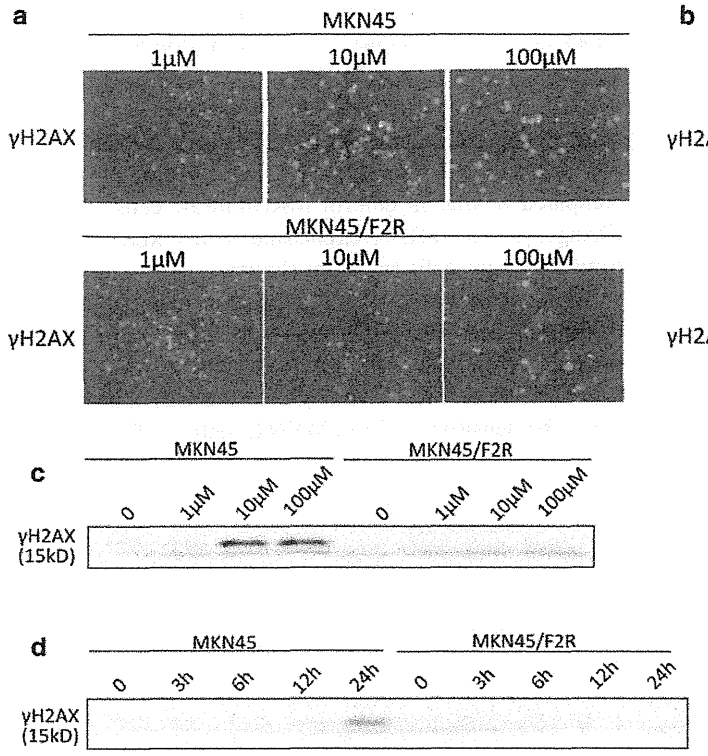

Fig. 3 The induction of double-strand breaks (DSBs) in MKN45 and MKN45/F2R cells after treatment with 5FU. An immunofluorescence analysis and a western blotting analysis for phosphor-H2AX, a DSB marker, were performed after treatment with the indicated concentrations of 5FU. **a** The results of the immunofluorescence analysis of MKN45 and MKN45/F2R cells treated with 5FU at concentrations of 1, 10, and 100 μM for 24 h. **b** The results of the immunofluorescence analysis of the MKN45 and MKN45/F2Rcells treated with 10 μM of 5FU for 3 h, 12 h, and 24 h. **c** The results of the western blotting analysis of MKN45 and MKN45/F2R cells treated with 5FU at concentrations of 1, 10, and 100 μM for 24 h. **d** The results of the western blotting analysis of MKN45 and MKN45/F2R cells treated with 10 μM of 5FU for 0, 3, 6,12, and 24 h

24 h compared to the control (Fig. 3c), and γH2AX was increased with 10 μM of 5FU in 24-h treatment compared with treatment for other periods (Fig. 3d).

MLH1 and PMS2 are linked to FANCJ after oxaliplatin treatment

The FANCJ/MutLα interaction is indispensable for ICL repair, and loss of FANCJ leads to failure of ICL repair [15]. To assess the interactions between these proteins and FANCJ after treatment in our cell lines, we performed co-immunoprecipitation studies.

After MKN45 cells were treated with 10 μM 5FU, 1 μM oxaliplatin,or both agents for 24 h, the cell lysates were immunoprecipitated with an anti-FANCJ antibody, and the presence of co-immunoprecipitated MLH1 and PMS2 was evaluated by a western blot analysis (Fig. 4). After the 5FU treatment, MLH1 and PMS2 were only minimally immunoprecipitated. However, after the oxaliplatin treatment, both MLH1 and PMS2 were immunoprecipitated to a greater extent than after the 5FU treatment, even though

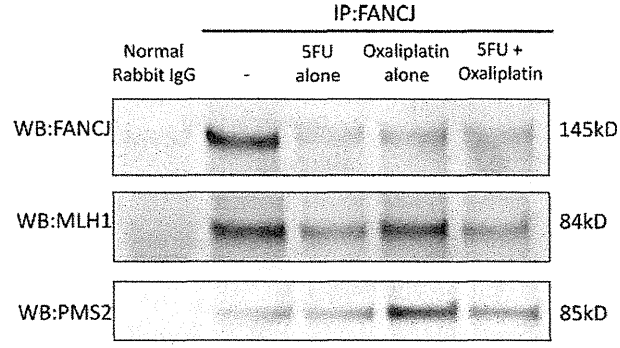

Fig. 4 Co-immunoprecipitation (*IP*) with an anti-FANCJ antibody. Co-immunoprecipitation of proteins with FANCJ after treatment of MKN45 cells with 10 μM 5FU and/or 1 μM oxaliplatin for 24 h. After oxaliplatin treatment, both MLH1 and PMS2 were immunoprecipitated to a greater extent than that after 5FU treatment alone, although the amount of FANCJ was decreased. *WB* Western blotting

the level of FANCJ decreased, suggesting that the amount of MutLα bound to FANCJ was increased after treatment with oxaliplatin in MKN45 cells.